SUPPLEMENTARY INFORMATION

Gas–Liquid Phase Equilibrium of a Model Langmuir Monolayer Captured by a Multiscale Approach

Ahmad Moghimikheirabadi*[1], Leonard M. C. Sagis[2], Martin Kröger[1], and Patrick Ilg[3]

[1]*Polymer Physics, Department of Materials, ETH Zurich, CH-8093 Zurich, Switzerland.*
[2]*Food Physics Group, Wageningen University, Bornse Weilanden 9, 6708 WG Wageningen, The Netherlands.*
[3]*School of Mathematical, Physical and Computational Sciences, University of Reading, Reading, RG6 6AX, UK.*

Contents

*Fax:+41 44 632 10 76; Tel: +41 44 633 92 32; E-mail: ahmad.moghimikheirabadi@mat.ethz.ch

1 3D reference simulations

1.1 Radial distribution functions of w-H and w-w pairs

As was discussed in the paper, w particles prefer H segments as neighbors over their own species. We verify this observation by calculating the radial distribution functions (rdf) of w-H and w-w pairs as given in Fig S1a. It is seen that the first peak in rdf is more pronounced for H-w pairs (solid line) and takes place at a smaller radial distance with respect to that of the w-w pairs (dash-dotted line). The average hydration number as a function of radial distance is calculated as

$$N_{\rm w}(r) = 4\pi\rho_w \int_0^r r'^2 g(r')dr', \tag{S1}$$

and presented in Fig. S1b for H and w particles. It clearly shows that for small radial distances (say less than 1.3σ), H segments have a larger hydration number than w particles.

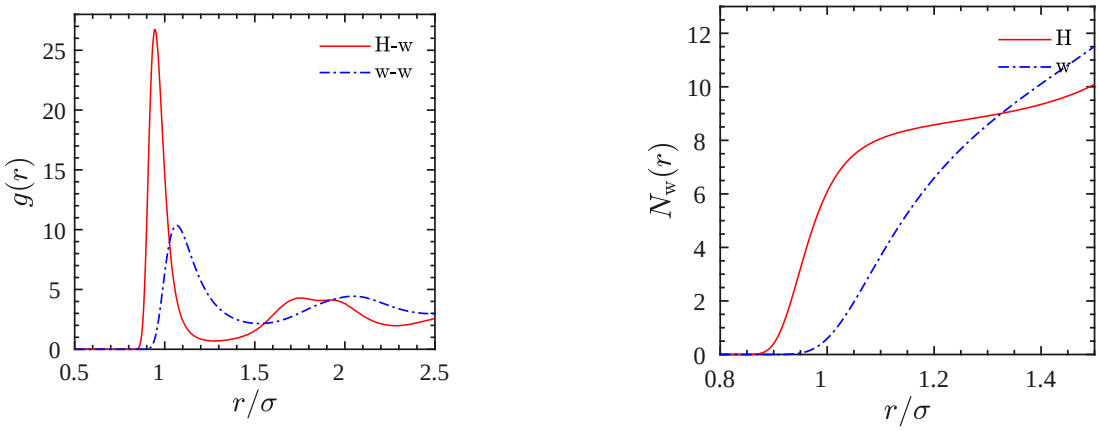

(a) **(b)**

Figure S1 (a) Pair correlation functions of H-w (solid line) and w-w (dash-dotted line) pairs. (b) Average number of neighboring w particles located until distance r, $N_{\rm w}(r)$, for H groups (solid line) and w (dash-dotted line) particles.

1.2 Force-matching scheme

In order to calculate the CG force field $F_{\rm CG}(r)$ numerically, we consider a cut-off distance r_c beyond which the radial force is assumed to be zero. The interval $[0, r_c]$ is meshed with equidistantly spaced grid points $\{r_i; i = 1, ..., \nu\}$ at $r_i/r_c = (i-1)/(\nu-1)$ so that $r_1 = 0$ and $r_\nu = r_c$. We consider a function space $\{f_i\}$ of linear spline basis functions[1,2] as

$$f_i(r) = \begin{cases} \frac{r-r_{i-1}}{r_i-r_{i-1}}, & r_{i-1} < r \leqslant r_i, \quad i > 1 \\ \frac{r_{i+1}-r}{r_{i+1}-r_i}, & r_i < r \leqslant r_{i+1}, \quad i < \nu \\ 0, & \text{otherwise}, \end{cases} \tag{S2}$$

and take $F_{\rm CG}(r)$ to be represented by ν coefficients $\{F_i\}$ as

$$F_{\rm CG}(r) = \sum_{i=1}^{\nu} F_i f_i(r). \tag{S3}$$

This representation implies that $F_{\rm CG}(r)$ is a piecewise continuous linear function, and the coefficients $\{F_i\}$ are the radial forces at the grid points $\{r_i\}$ as

$$F_i = F_{\rm CG}(r_i), \tag{S4}$$

subjected to the boundary condition of $F_\nu = 0$. In the following, we discuss how to calculate coefficients $\{F_i\}$ by matching the forces in the CG system with the reference system through minimizing the residual $\chi^2(\mathbf{F})$. By

plugging Eq. S3 into Eq. 15, we rewrite the CG force $\mathbf{F}_I$ in terms of coefficients $\{F_i\}$ as

$$\mathbf{F}_I = \sum_{i=1}^{\nu} F_i \mathbf{a}_{iI}, \tag{S5}$$

where

$$\mathbf{a}_{iI} = \sum_{J=1,\neq I}^{N_{\text{int}}} f_i(|\mathbf{R}_I - \mathbf{R}_J|) \frac{\mathbf{R}_I - \mathbf{R}_J}{|\mathbf{R}_I - \mathbf{R}_J|}, \tag{S6}$$

is known since it is only dependent on projected surfactant center-of-masses and the function space $\{f_i\}$. Combining Eqs. S5 and 15 results in a linear least-squares problem as

$$\chi^2(\{F_i\}) = \left\langle \frac{1}{2N_{\text{int}}} \sum_{I=1}^{N_{\text{int}}} \left| \sum_{i=1}^{\nu} F_i \mathbf{a}_{iI} - \mathbf{f}_I \right|^2 \right\rangle, \tag{S7}$$

where the coefficients $\{F_i\}$ are to be determined numerically. To this end, we solve equivalently an overdetermined linear system of equations[2–4] obtained by equalizing x and y components of the total force ($\mathbf{f}_I$) exerted on each surfactant center-of-mass at each reference configuration with the corresponding CG force ($\mathbf{F}_I$) in terms of fitting coefficients $\{F_i\}$. After some trial and errors, we set the cut-off distance to $r_c = 10\sigma$ (not to be confused with r_{cut} in the manuscript) and consider a nonuniform radial mesh with 358 grid points as $\{r_i/\sigma\} = \{0, 1.1, 1.125, ..., 9.975, 10\}$. We note that intermolecular distances with very small separation (say less than 1.1σ in our cases) are rarely sampled, and hence one can not accurately estimate the value of the forces $\{F_i\}$ in this region. That is why we have considered only one coarse mesh in the interval $[0, 1.1]$ and safely assumed[1] $F_1 = F_2$. We approximate the solution in a block-averaging[1] approach where we partition configurations into disjoint blocks each of which consists roughly of 80000 equations (e.g. for a simulation consisting of 400 surfactants, 50 blocks with the size of 100 each). We then solve the overdetermined linear system of equations in each block by using the LSQR[5,6] algorithm and subsequently average the results of $\{F_i\}$ over different blocks.

2 Gibbs ensemble Monte Carlo (GEMC)

2.1 Particle displacement

To sample equilibrium configurations within each simulation box we perform displacements of randomly selected particles in a randomly selected region according to the following acceptance probability[7,8]

$$\mathscr{P}_{\text{disp},\kappa} = \min\left(1, \exp[-\beta \Delta U^{\kappa}_{\text{disp}}]\right), \quad \kappa = \{le, g\} \tag{S8}$$

where $\Delta U^{\kappa}_{\text{disp}}$ denotes the change in the internal energy of phase κ due to the particle displacement.

2.2 Area exchange

For the area change trial moves, we perform a random walk in $\ln(A^l/A^g)$ with the acceptance probability $\mathscr{P}_{\text{area}}$, described by[7]

$$\mathscr{P}_{\text{area}} = \min\left(1, \left(\frac{A^{le} + \Delta A}{A^{le}}\right)^{N^{le}+1} \left(\frac{A^g - \Delta A}{A^g}\right)^{N^g+1} \exp\left[-\beta\left(\Delta U^{le}_{\text{area}} + \Delta U^{g}_{\text{area}}\right)\right]\right), \tag{S9}$$

where ΔA is the area change in region le (and hence $-\Delta A$ is the area change in region g) and $\Delta U^{\kappa}_{\text{area}}$, $\kappa = \{le, g\}$, is the change in the internal energy of phase κ associated with that area change. These trial moves result in the pressure equality of the two coexisting phases.

2.3 Particle exchange

Finally, we transfer a randomly selected particle from a randomly selected phase to the other to ensure the chemical equilibrium between two coexisting regions. The acceptance probability of removing a particle from phase le, and inserting that in phase g is given by[7,8]

$$\mathscr{P}_{\rm ex} = \min\left(1, \frac{N^{le}A^{g}}{(N^{g}+1)A^{l}} \exp\left[-\beta\left(\Delta U^{le}_{\rm ex} + \Delta U^{g}_{\rm ex}\right)\right]\right) \tag{S10}$$

where $\Delta U^{\kappa}_{\rm ex}$, $\kappa = \{le, g\}$, is the change in the internal energy of box κ associated with the particle insertion for g and particle removal for le phases.

2.4 Implementation details

We considered two periodic simulation boxes each with initial dimensions as $50\sigma \times 50\sigma$. A total number of 500 particles are equally distributed between the two boxes. For each MC step, we perform 500 particle displacements (with the acceptance rate of $40 \pm 5\%$), 10 area change and 10 particle exchange trial moves in a random order. For the first 5×10^4 steps, we only perform particle displacements within the individual boxes without any area change or particle exchange moves. Subsequently, we perform 1.5×10^5 full MC steps, including particle exchange and area change moves. During this interval, we monitor the densities in the two boxes to make sure they are constant (but with a different value at each box, in case of coexistence) within the statistical fluctuations. Finally, we sample equilibrium configurations once every 20 steps for the next 10^5 MC steps.

3 Density functional theory (DFT)

In this section, we discuss different building blocks of our 2D DFT approach, and the numerical methods for calculating coexistence properties, density profiles across the G-LE dividing line and the corresponding line tensions.

3.1 Chemical potential of the hard-disc fluid

To obtain an expression for the chemical potential of the hard-disc fluid, and hence its free energy, we write down the Gibbs-Duhem relation for a constant temperature process as[9]

$$d\Pi_{\rm hd} = \rho d\mu_{\rm hd}, \quad T = \text{cst.} \tag{S11}$$

Subtracting the same equation applied to an ideal gas at the same density, multiplying by $\beta = 1/k_{\rm B}T$ and dividing by $d\rho$ results in

$$\left.\frac{\partial \beta\mu^{\rm ex}_{\rm hd}}{\partial\rho}\right|_{T} = \frac{1}{\rho}\left.\frac{\partial \beta\Pi^{\rm ex}_{\rm hd}}{\partial\rho}\right|_{T} \tag{S12}$$

where $p^{\rm ex}_{\rm hd}$ and $\mu^{\rm ex}_{\rm hd}$ are excess properties of the hard-disc fluid. By using the ideal gas law and the hard-disc equation of state[10] (Eq. 29), we obtain $\beta p^{\rm ex}_{\rm hd}$ as

$$\beta\Pi^{\rm ex}_{\rm hd}(\rho) = \beta\Pi_{\rm hd} - \beta\Pi^{\rm id}_{\rm hd} = \frac{\rho}{(1-\eta)^2} - \rho, \qquad \eta = \frac{\pi}{4}\rho d^2. \tag{S13}$$

Integrating Eq. S12, we obtain

$$\beta\mu^{\rm ex}_{\rm hd}(\rho) - \beta\mu^{\rm ex}_{\rm hd}(\rho_0) = \int_{\eta_0}^{\eta} \frac{1}{\eta'}\left(\frac{\partial \beta\Pi^{\rm ex}_{\rm hd}}{\partial\rho'}\right)_{T} d\eta', \tag{S14}$$

and by replacing Eq. S13 into this integral we get

$$\beta\mu^{\rm ex}_{\rm hd}(\rho) - \beta\mu^{\rm ex}_{\rm hd}(\rho_0) = \left[-\ln(1-\eta) + \frac{1}{1-\eta} + \frac{2\eta-\eta^2}{(1-\eta)^2}\right]_{\eta_0}^{\eta}. \tag{S15}$$

In the limit where $\rho_0 \to 0$ (and hence $\eta_0 \to 0$), the hard-disc fluid behaves like an ideal gas and $\beta\mu_{\rm hd}^{\rm ex}(\rho_0) \to 0$, therefore the excess chemical potential can be evaluated from Eq. S15 as

$$\beta\mu_{\rm hd}^{\rm ex}(\rho) = -\ln(1-\eta) + \frac{3\eta - 2\eta^2}{(1-\eta)^2}. \tag{S16}$$

Finally, the full chemical potential is obtained by adding the ideal gas contribution and then reads

$$\beta\mu_{\rm hd}(\rho) = \beta\mu_{\rm hd}^{\rm ex}(\rho) + \beta\mu_{\rm hd}^{\rm id}(\rho) = \ln\Lambda^2\rho - \ln(1-\eta) + \frac{3\eta - 2\eta^2}{(1-\eta)^2}, \tag{S17}$$

where Λ is the thermal de Broglie wavelength.

3.2 Coefficient α and disc diameter d

The coefficient α is calculated as $21.43 \pm 0.74\,\varepsilon\sigma^2$ by using tabulated values of $U^{\rm att}(r)$ and carrying out the following integral by using the trapezoidal rule

$$\alpha = -\int_0^{r_c} 2\pi r U^{\rm att}(r) dr, \tag{S18}$$

with r_c from above. Similarly, $d_{\rm BH}(T)$ is numerically calculated from Eq. 27 by using tabulated values of the repulsive branch of the interaction potential $U^{\rm rep}(r)$, and its values at different temperatures are shown in Fig. S2.

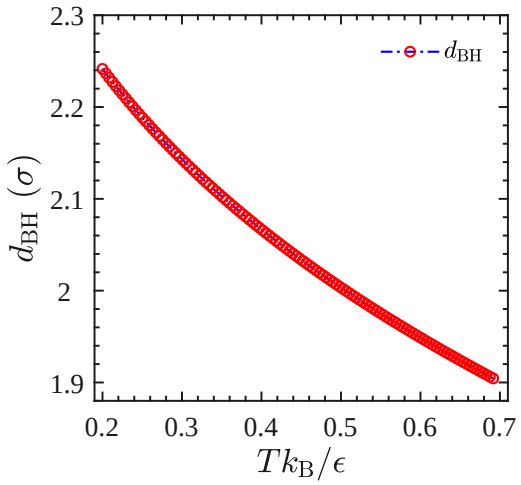

Figure S2 Hard disc diameter, $d_{\rm BH}(T)$, for 2D fluid of surfactant center-of-masses at different temperatures.

3.3 Coexistence properties and phase diagram

To calculate the coexisting densities ρ_g^* and ρ_l^* at given T we basically follow the procedure described earlier by us in another context.[11] Within the region of coexistence the spinodal equation, following from Eq. 34 (etc.)

$$\frac{d^2 f}{d\rho^2} = \frac{d\mu}{d\rho} = \frac{16 k_{\rm B} T}{\rho} \frac{(4 + \pi d^2 \rho)}{(4 - \pi d^2 \rho)^3} - \alpha = 0 \tag{S19}$$

can be solved analytically for two spinodal densities $\rho_g^{\rm spi} < \rho_{le}^{\rm spi}$. The value for the chemical potential we are looking for must assume this value at some yet to be determined ρ^* located between the spinodal densities. Because pressures and chemical potentials are identical for the coexisting states (binodal), the desired $\rho^* \in [\rho_g^{\rm spi}, \rho_{le}^{\rm spi}]$ has the feature – known as Maxwell's construction – that a net area ΔI in the μ–ρ–diagram vanishes. More formally,

$$\Delta I(\rho^*) \equiv I_-(\rho^*) - I_+(\rho^*) = 0 \tag{S20}$$

with partial areas defined by

$$I_-(\rho^*) = \int_0^{\rho^*} \max[0, \mu(\rho) - \mu(\rho^*)] d\rho, \tag{S21}$$

$$I_+(\rho^*) = \int_{\rho^*}^{1} \max[0, \mu(\rho^*) - \mu(\rho)]\, d\rho \tag{S22}$$

Calculating ρ^* thus amounts to finding the root of a known scalar function $\Delta I(\rho^*)$ of a single variable ρ^*, which is computationally inexpensive. Since $I_-(\phi_g^{\rm spi}) = I_+(\phi_{le}^{\rm spi}) = 0$ and $I_-(\phi_{le}^{\rm spi}) > 0$ and $I_+(\phi_g^{\rm spi}) > 0$, there is exactly one such root $\rho^* \in [\rho_g^{\rm spi}, \rho_{le}^{\rm spi}]$. With this root ρ^* at hand we know the value of the chemical potential in the coexisting phases, $\mu_\kappa^* \equiv \mu(\rho_\kappa^*) = \mu(\rho^*)$ for $\kappa \in \{g, le\}$, and herefrom the coexisting densities ρ_κ^* as well. The pressures $p_\kappa^* = p(\rho_\kappa^*)$ are identical by construction, because

$$\begin{aligned} \Pi_g^* - \Pi_{le}^* &= -f(\rho_g^*) + \rho_g^* \mu_g^* + f(\rho_{le}^*) - \rho_{le}^* \mu_{le}^* \\ &= \int_{\rho_g^*}^{\rho_{le}^*} \mu(\rho)\, d\rho - (\rho_{le}^* - \rho_g^*)\mu(\rho^*) = \Delta I(\rho^*) = 0 \end{aligned} \tag{S23}$$

actually proving and hereby employing the Maxwell construction of equal areas I_- and I_+.

3.4 Density profile and line tension

For a given T, the value of the chemical potential at coexistence, $\mu \equiv \mu_{le}^* = \mu_g^*$, will be used to solve Eq. 43, which we repeat here as

$$\mu_{\rm hd}(\rho^{i+1}(y)) = \mu - \int d\mathbf{r}' U^{\rm att}(|\mathbf{r} - \mathbf{r}'|)\rho^i(y'). \tag{S24}$$

We consider a semi-infinite rectangular domain in the xy-plane, with a length of $y_{\max} = 100\sigma$ in the y-direction and a very large length ($L \to \infty$) in the x-direction. For a spherically symmetric potential $U^{\rm att}(r)$ with a cut-off r_c, Eq. S24 can be written as

$$\mu_{\rm hd}(\rho^{i+1}(y)) = \mu - \int_0^{2\pi} \int_0^{r_c} r' U^{\rm att}(r') \rho^i(y + r' \sin\theta) dr' d\theta. \tag{S25}$$

We mesh the interval $[0, y_{\max}]$ with 201 equally spaced grid points in the y-direction (and hence resolve the density profile in this region). For the regions beyond this domain, which correspond to the gas and liquid bulk phases with uniform densities, we assume

$$\begin{cases} \rho(y) = \rho(0), & y < 0 \\ \rho(y) = \rho(y_{\max}), & y > y_{\max}. \end{cases} \tag{S26}$$

The iterations are then started by a nonuniform density profile, e.g. half of the grid points taking the value of ρ_l and the other half ρ_g. For each grid point y_j, the double integral in the right-hand-side (RHS) of Eq. S25 is evaluated (by knowing ρ^i profile from the previous iteration) numerically using trapezoidal method where we considered 101 grid points in the r-direction (to mesh the interval $[0, r_c]$) and 51 grid points in the θ-direction. The values of $\mu_{\rm hd}(\rho^{i+1}(y_j))$ are then used to solve Eq. 30 for $\rho^{i+1}(y_j)$. We continue iterations until meeting the stopping criterion as

$$\int_0^{y_{\max}} \left(\rho^{i+1}(y) - \rho^i(y)\right)^2 dy \;\le\; 10^{-6} \int_0^{y_{\max}} \rho^i(y)^2 dy, \tag{S27}$$

and denote the converged density profile as $\rho(y)$. We note that the convergence was achieved in our cases with roughly 7 iterations.

The grand potential, Ω, we calculate using this $\rho(y)$, and performing the integral in Eq. 45 over the 2D domain as

$$\Omega = L \int_0^{y_{\max}} [f_{\rm hd}(\rho(y)) - \mu\rho(y)] dy + \frac{L}{2} \int_0^{y_{\max}} g(y)\rho(y) dy, \tag{S28}$$

where $g(y)$ is the integral on the right hand side of Eq. S25, i.e.,

$$g(y) = \mu - \mu_{\rm hd}(\rho(y)). \tag{S29}$$

The line tension γ_{line} simply follows from Eq. 46 as

$$\gamma_{\text{line}} = \frac{\Omega}{L} + \Pi y_{\text{max}}. \tag{S30}$$

where $\Pi \equiv \Pi^*_{le} = \Pi^*_g$ is the pressure of the coexisting phases.

References

1 W. G. Noid, P. Liu, Y. Wang, J.-W. Chu, G. S. Ayton, S. Izvekov, H. C. Andersen and G. A. Voth, *J. Chem. Phys.*, 2008, **128**, 244115.

2 A. Moghimikheirabadi, L. M. C. Sagis and P. Ilg, *Phys. Chem. Chem. Phys.*, 2018, **20**, 16238–16246.

3 S. Izvekov and G. A. Voth, *J. Phys. Chem. B*, 2005, **109**, 2469–2473.

4 S. Izvekov and G. A. Voth, *J. Chem. Phys.*, 2005, **123**, 134105.

5 C. C. Paige and M. A. Saunders, *ACM Trans. Math. Softw.*, 1982, **8**, 43–71.

6 C. C. Paige and M. A. Saunders, *ACM Trans. Math. Softw.*, 1982, **8**, 195–209.

7 D. Frenkel and B. Smit, in *Understanding Molecular Simulation*, Academic Press, San Diego, 2nd edn., 2002, pp. 201–224.

8 A. Z. Panagiotopoulos, *Mol. Phys.*, 1987, **61**, 813–826.

9 I. Kusaka, in *Statistical Mechanics for Engineers*, Springer International Publishing, 2015, pp. 259–308.

10 E. Helfand, H. L. Frisch and J. L. Lebowitz, *J. Chem. Phys.*, 1961, **34**, 1037–1042.

11 A. Halperin and M. Kröger, *Macromolecules*, 2011, **44**, 6986–7005.